Optics Letters

Integration of cascaded electro-optic and nonlinear processes on a lithium niobate on insulator chip

TINGTING DING,[1,2] YUANLIN ZHENG,[1,2,3] AND XIANFENG CHEN[1,2,4]

[1]State Key Laboratory of Advanced Optical Communication Systems and Networks, School of Physics and Astronomy, Shanghai Jiao Tong University, Shanghai 200240, China
[2]Key Laboratory for Laser plasma (Ministry of Education), Collaborative Innovation Center of IFSA (CICIFSA), Shanghai Jiao Tong University, Shanghai 200240, China
[3]e-mail: ylzheng@sjtu.edu.cn
[4]e-mail: xfchen@sjtu.edu.cn

Received 11 January 2019; accepted 15 February 2019; posted 19 February 2019 (Doc. ID 357471); published 15 March 2019

Cascading of the electro-optic (EO) effect and nonlinear wave mixing can provide a way to manipulate photonic conversion in an electrically controllable manner. Here we experimentally demonstrate simultaneous transverse EO coupling and second-harmonic generation (SHG) in a periodically poled lithium niobate on insulator ridge waveguide. With tight light confinement, large EO, and nonlinear coefficients in the LNOI waveguide, the integrated device features a low-voltage fast-speed response for EO coupling and efficient conversion for SHG. The proposed scheme holds promise in realizing electrically controllable on-chip nonlinear devices.

https://doi.org/10.1364/OL.44.001524

Cascading of wave-mixing processes plays an important role in optics through which one can achieve complex manipulation or highly enhanced conversion of photons beyond a direct process. The concept has been implemented in a vast range of applications in both classical and quantum optics. One significant example is the cascaded $\chi^{(2)}:\chi^{(2)}$ effect to achieve an enhanced effective $\chi^{(3)}$ nonlinearity. This has often been exploited for flexible frequency conversion applications [1,2]. Other prominent applications taking the advantages of cascading include large nonlinear phase shift generation [3,4], all-optical switching [5], cascaded four-wave mixing [6], and terahertz generation [7]. Many experiments, such as high-order harmonic generation [8,9] and frequency comb generation [10,11], are also the involvement of cascading processes.

Among these, the cascading of the electro-optic (EO) effect and nonlinear wave mixing is of significance for enhancement or control of the optical process with a simple method of applying voltages. For instance, the cascading of EO and optical rectification effect can lead to an effective Kerr nonlinearity in noncentrosymmetric materials without the need for phase matching [12]. Cascaded EO and non-phase matched SHG was achieved to establish a positive or negative lensing effect with a large effective nonlinear refractive index [13]. The cascaded EO effect and second-order nonlinearity have also been proposed to demonstrate optical bistability in periodically poled lithium niobate (PPLN) [14]. It has also been proposed that the enhanced nonlinear EO effect (Kerr effect) effectively modifies the phase matching of SHG and, thus, controls the process [15].

Despite important and promising, previous proposals and demonstrations suffer from inefficiency in both sub-processes in bulk structures. This issue is crucial if actual applications are to be achieved. The solution is to realize the scheme in photonic integrated circuits, e.g., waveguide structures, in which both EO coupling and nonlinear wave mixing can be dramatically enhanced. The emerging technology of lithium niobate on insulator (LNOI) [16] has provided an ideal platform for such a purpose. A variety of important functionalities has already been realized, such as high-speed EO modulators [17–19] in linear optics, and frequency converters [20–22] in nonlinear optics. The LNOI platform is ideal for both electrical and nonlinear device implementations, and for the combination of the two.

In this Letter, we report the realization of simultaneous transverse EO coupling and second-harmonic generation (SHG) in a periodically poled lithium niobate on insulator (PPLNOI) ridge waveguide on the LNOI platform. The integration of the cascading process is demonstrated at a low-voltage fast-speed drive for EO coupling and a relatively low input power for SHG. The demonstration shows a new type of on-chip functionality on the LNOI platform, which implies one step further towards on-chip dynamic control of nonlinear wave mixing.

Figure 1(a) schematically shows the proposed cascaded EO coupling and SHG process on a PPLNOI chip. The cascading process involves simultaneous first-order quasi-phase-matched (QPM) o-e polarization coupling and ee-e (type 0) SHG processes. The dimension of the PPLNOI waveguide in our experiment is 6.0 μm(W) × 5.0 μm(T) × 10 mm. The ridge waveguide, which is between two parallel 2.5-μm deep grooves, is fabricated in a chemo-mechanically thinned PPLN layer (5.0 μm thick) using optical grade dicing [23,24]. The poling

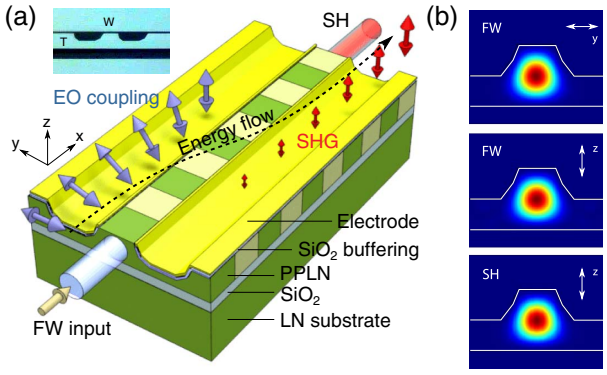

Fig. 1. (a) Schematic of the cascading EO coupling and SHG process in the PPLNOI ridge waveguide. The inset is the cross-sectional image of the used LNOI chip in our experiment. (b) Calculated fundamental mode profiles of the FW (1590 nm) and SH (795 nm) in the PPLNOI ridge waveguide. The arrows indicate the polarization direction of the optical field.

period, Λ, of the PPLN layer is 20.5 μm, and the duty cycle is 50%. A Silica layer (estimated to be several hundred nanometers thick) is evaporated on top for buffering. Then metallic (Ni/Cr) electrodes of 50 nm thick are deposited on both side walls for voltage applying. The optical axis is along the z axis. Light propagates in the ridge waveguide along the x axis, and a transverse electric field is along the y axis.

The considered cascading steps involve $\omega_{1y} \rightarrow \omega_{1z}$ (transverse EO coupling) and $\omega_{1z} + \omega_{1z} \rightarrow \omega_{2z}$ (type-0 SHG). The simultaneous first-order QPM condition for these two processes can be reached in the telecom wavelengths in PPLN. The two wavevector mismatches are $\Delta k_{\mathrm{EO}} = k_{1y} - k_{1z} - G$ and $\Delta k_{\mathrm{SHG}} = 2k_{1z} - k_{2z} - G$, respectively. $k_j = 2n_j\pi/\lambda_j$ are wavevectors of the interacting waves with subscripts $j = 1, 2$ referring to the fundamental wave (FW) and SH, and y, z referring to the polarization direction, respectively. n_j is the refractive index of each wave and should be replaced by the effective refractive index in waveguide structures. $G = 2m\pi/\Lambda$ is the reciprocal vector of the QPM structure with m is the order of QPM, and Λ is the poling period of PPLN.

The cascading process occurs under the simultaneous QPM condition, when both transverse EO coupling and SHG processes are momentum compensated for in the PPLNOI waveguide. The cascading effect can also be well understood based on a simplified modeling of plane wave approximation. The coupling equations governing the wave mixing can be written as [25,26]

$$\begin{cases} \frac{dA_{1y}}{dx} = -i\beta A_{1z} e^{i\Delta k_{\mathrm{EO}} x}, \\ \frac{dA_{1z}}{dx} = -i\beta A_{1y} e^{-i\Delta k_{\mathrm{EO}} x} - i\kappa A_{2z} A_{1z}^{*} e^{-i\Delta k_{\mathrm{SHG}} x}, \\ \frac{dA_{2z}}{dx} = -\frac{1}{2} i\kappa A_{1z}^{2} e^{i\Delta k_{\mathrm{SHG}} x}. \end{cases} \quad (1)$$

Here A is the normalized complex amplitude of the wave. The coupling coefficients are $\beta = -\gamma_{51} f_a \omega_1 E_y/(2c) \cdot \sqrt{n_{1y}^3 n_{1z}^3}$ and $\kappa = d_{33} f_b / c \cdot \sqrt{\omega_1^2 \omega_2 / (n_{1z}^2 n_{2z})}$. E_y is the transverse electric field intensity. d_{33} and γ_{51} are the effective nonlinear and EO coefficients, respectively. $f_a = f_b = 2/\pi$ are the Fourier coefficients associated with the first-order reciprocal vector ($G = 2\pi/\Lambda$) when the duty ratio is 0.5. ω is the angular frequency of the optical wave, n is the refractive index, x is the interaction distance along the light propagation direction (x axis), and c is the speed of light in vacuum. Equation (1) is used in our numerical simulation for cascading processes in the waveguide structure. The only difference is that the refractive index is rendered as an effective one due to structural dispersion of the waveguide structure, and needs case-to-case calculation.

Figure 2 shows the e-polarized SH output ($|A_{2z}|^2$) for different FW input and varied applied electric field intensities. The QPM condition ($\Delta k_{\mathrm{OE}} = \Delta k_{\mathrm{SHG}} = 0$) is assumed in the simulation. The interaction length is set to be 10 mm. The SH intensity always follows a quadratic relation with respect to the input for both polarization states, while its response to the transverse electric field is more complex. Still, the results show the ability to electrically control the SHG process. The advantage for integration on the LNOI platform is that both the electrical field per voltage and optical field can be simultaneously boosted, leading to low-voltage drive and enhanced nonlinear conversion. The realization of on-chip electrically controlled nonlinear devices, thus, can be straightforward.

As shown in Fig. 3(a), light from a telecom band CW tunable laser (spectral range: 1520–1600 nm) and amplified by an erbium doped fiber amplifier is used as the source for the FW. Its polarization is controlled using a polarization controller (PC). An in-line polarization beam splitter (PBS) and a segment of polarization maintaining (PM) fiber are used to guarantee linear polarization of the input. The FW is controlled to be either e- or o-polarized with respect to the ridge PPLNOI waveguide. The FW is coupled into the ridge waveguide via the pigtail end of the PM fiber glued to the PPLNOI chip. The output of the ridge waveguide is collimated in free space by a lens. The inset image is the photograph of the package of our device (in collaboration with *HC Photonics Corp.*), corresponding to the setup within the dashed rectangle marked in the schematic illustration.

First, the characteristics of EO coupling and SHG processes are separately investigated. The EO coupling is investigated under the Solc-type filtering configuration by placing an orthogonal polarizer and detecting the FW transmission. The half-wave voltage of the transverse EO coupling is measured to be 13 V, while a theoretical prediction of the value is 5.4 V (or 0.9 V/μm). The type-0 QPM SHG is investigated by input e-polarized FW utilizing the largest nonlinear coefficient (d_{33}) of LN. The output is collected using a focusing lens and a

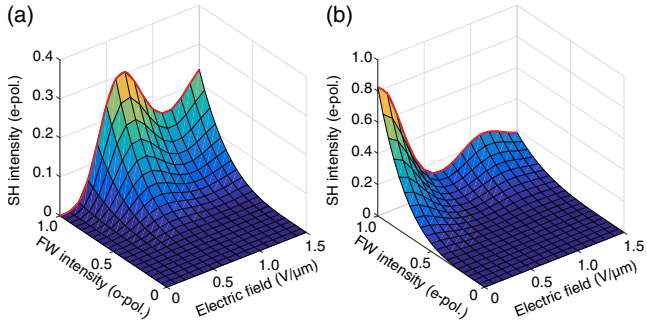

Fig. 2. Simulation of SH output ($|A_{2z}|^2$) with respect to the FW power and transverse voltage of the cascading process for (a) the o-polarized FW input, A_{1y}, and (b) the e-polarized FW input, A_{1z}.

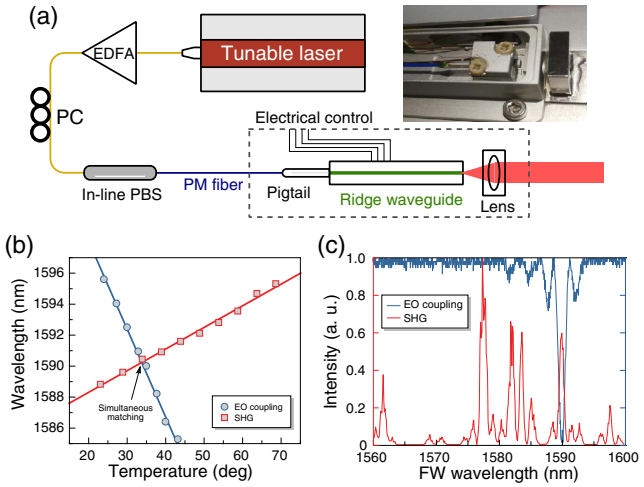

Fig. 3. (a) Schematic illustration of the experimental setup. (b) Experimentally measured QPM conditions for both EO coupling and SHG. The intersect point of the lines is the condition of simultaneous QPM for the cascading process. (c) Measured phase-matching spectra for EO coupling (measured under a Solc-type filtering configuration) and SHG overlapping at T = 34.7°C.

multimode fiber to spectral analyzers. The generated SH signal is monitored, while the FW wavelength is swept. Figure 3(b) shows the experimentally measured QPM wavelengths for both EO coupling and SHG in the PPLNOI ridge waveguide. The tuning slopes of EO coupling and SHG are −0.54 nm/°C and 0.16 nm/°C, respectively. The found condition for both wave mixing processes to cascade is when the wavelength of the FW is set at 1590.2 nm, and the temperature is set at 34.7 deg. The QPM wavelength for both EO coupling and SHG shows good linear relation on the device temperature. The bandwidths at full width at half-maximum) are 1.6 and 0.8 nm at the simultaneous QPM condition for EO coupling and SHG, respectively, as shown in Fig. 3(c). The theoretical function has the form of $\mathrm{sinc}^2(\Delta kL/2)$, where Δk is the wavevector mismatch, and L is the interaction distance or the waveguide length. SHG has a narrower QPM bandwidth due to stronger dispersion between the FW and SH waves.

It should be noted that the ridge waveguide is multimode, i.e., supports multiple eigenmodes, due to a relatively large cross section and high refractive index contrast. In our experiment, only one QPM condition for EO coupling was found within the laser's tunable range, while SHG occurred at multiple FW wavelengths. This is because the input excites one fundamental spatial mode, and mode coupling between the fundamental TE and TM modes is allowed. The fundamental (or first order) and higher-order modes are either inefficient in overlapping or phase mismatched within the scanning range. At the SH wavelength, however, the mode density is much more dense, and the QPM can be occasionally achieved between the FW and different spatial orders of SH modes. The SHG between fundamental spatial modes of the FW and SH is estimated to be beyond 1600 nm, outside the laser scanning range, which would exhibit much higher conversation efficiency.

For EO coupling, we can modulate the coupling dynamics at a 3 dB bandwidth of approximately 125 MHz, with the peak response at 70 MHz. The frequency response is shown in

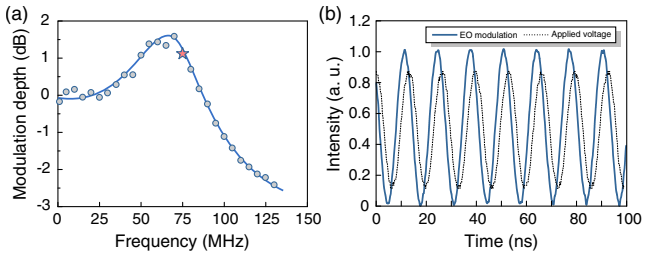

Fig. 4. (a) Small-signal EO response of the device. (b) EO modulated FW output of the device at 75 MHz.

Fig. 4(a). Figure 4(b) shows the modulation at 75 MHz, which recovers the modulated intensity of the output optical field. This shows the efficient mode conversion and the relatively fast-speed operation capability of our device for EO coupling. This has been well investigated, and more details can be found in our previous work [27].

For QPM SHG, the FW input is set to be e-polarized (A_{1z}) without applying any voltage signal. The spatial output of the device is focused into a multimode fiber and analyzed using spectrometers. The spectrum is shown in Fig. 5(a); the inset is the recorded FW mode profile in the far field in free space. At the cascading condition, SH at 795 nm was observed with a peak conversion efficiency with the FW at 1590.2 nm. A wider spectral linewidth of SH attributes to the lower resolution of the VIS/NIR fiber spectrometer. Figure 5(b) shows the collected SH intensity at the increased FW power from the fiber port. The converted SH intensity has a quadratic power dependence on that of the FW, which agrees well with the theoretical prediction. Considering the device transmission efficiency (45%) and SH collection efficiency (10%), the normalized conversion efficiency in the ridge waveguide is approximately 4×10^{-4} $\mathrm{W^{-1}\,cm^{-2}}$. The performance is lower than the theoretical upper limit and those reported by other research groups [20,28,29]. This is due to a poor mode overlapping for the FW mode and higher spatial order of SH. Higher conversion efficiency can be expected in the waveguide with a smaller cross section and more proper QPM period to guarantee phase matching between the fundamental spatial order of the two modes.

One important aspect of cascading of EO coupling and nonlinear wave mixing is the capability of simple electrical control of photonic manipulation/conversion, which holds promise for novel on-chip functionalities in integrated nonlinear and quantum optics. To show the electrical controlling capability of the

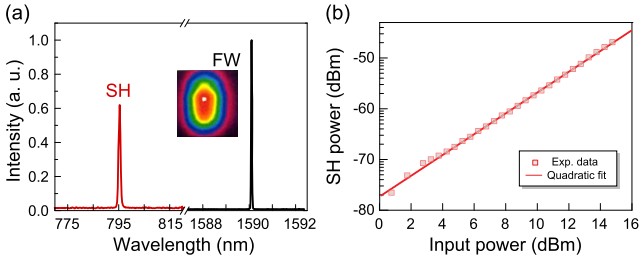

Fig. 5. (a) Spectrum of the respective FW and SH waves (not to scale). The inset is the recorded intensity profile of the output FW in free space. (b) Collected SH power as a function of the FW input. The fitting line has a slope of 2.

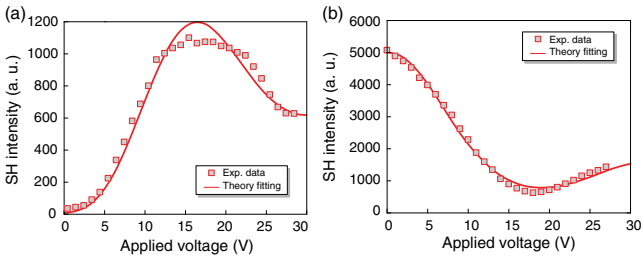

Fig. 6. Output SH intensity ($|A_{2z}|^2$) versus the applied voltage with (a) the o-polarized FW input (A_{1y}) and (b) the e-polarized FW input (A_{1z}).

cascading process, we measured the output SH intensity, $|A_{2z}|^2$, by applying different DC voltages to trigger EO coupling and the consequent SHG. The FW wavelength is 1590.2 nm with the device temperature maintained at 34.7°C to guarantee the cascading condition. The SH output is monitored using the calibrated spectrometer, which has high sensitivity, but slow response. Successful cascading can be directly observed when the SH output signal is strong and varied with the changing voltage. Figure 6 shows the electrical control dynamics of SHG by the applied voltage at a constant input power. The SH intensity is recorded on the applied voltage for both o- and e-polarized FW input at 10 mW, as shown in Figs. 6(a) and 6(b). The solid lines are theoretical fitting according to the numerical simulation (see Fig. 2). The experimental results fit well with those of the numerical simulation. As can be seen, the subsequent SHG can be controlled with applied voltage; that is, the electrical control of SHG via the cascading on the LNOI chip is demonstrated. One should note that the SH intensity does not reach zero in the case in which the FW input is e-polarized. Thus, the o-polarized FW input scheme may be more favorable for the demonstration of devices for higher contrasts.

Fast-speed control of the cascading process can be done by applying a high-frequency AC electric field along the transverse direction. Due to our experimental constraints, the generated SH intensity was still not high enough to be directly measured using high-speed detectors, which have lower sensitivity and typically require an average power over −30 dBm or μW scale. The modulation of the EO effect at the FW wavelength indirectly shows the control of the cascaded SHG at the same speed. Still, we succeed to demonstrate integration of a cascading process on the LNOI platform, achieving an EO tunable SHG converter for low drive voltage and weak optical input. This provides a novel way for manipulation of nonlinear photonics on a chip via a simple manner, i.e., by electrical controlling. In particular, with LNOI nano waveguides [18,19,22,30], the overall performance of the device can be dramatically improved. Since LN is highly anisotropy, and its optical properties (both linear and nonlinear) are polarization sensitive, the cascading of EO coupling and nonlinear wave mixing can be expected to exhibit more applications on the integrated LNOI platform.

In conclusion, we have demonstrated the integration of cascading process of EO coupling and SHG in the PPLNOI ridge waveguide, presenting an electrically controllable nonlinear conversion on the LNOI platform. The configuration offers avenues to manipulate nonlinear wave mixing through an EO effect on a chip. The scheme holds promise for realizing electrically controllable on-chip nonlinear devices.

Funding. National Natural Science Foundation of China (NSFC) (11604206, 11734011); National Key R&D Program of China (2017YFA0303701, 2018YFA0306301); Foundation for Development of Science and Technology of Shanghai (17JC1400400).

REFERENCES

1. M. Ahlawat, A. Tehranchi, K. Pandiyan, M. Cha, and R. Kashyap, Opt. Express **20**, 27425 (2012).
2. R. Wolf, I. Breunig, H. Zappe, and K. Buse, Opt. Express **25**, 29927 (2018).
3. G. I. Stegeman, M. Sheik-Bahae, E. V. Stryland, and G. Assanto, Opt. Lett. **18**, 13 (1993).
4. G. I. Stegeman, D. J. Hagan, and L. Torner, Opt. Quantum Electron. **28**, 1691 (1996).
5. R. Schiek, Y. Baek, G. Krijnen, G. I. Stegeman, I. Baumann, and W. Sohler, Opt. Lett. **21**, 940 (1996).
6. A. C. S. Jr., J. M. C. Boggio, A. A. Rieznik, H. E. Hernandez-Figueroa, H. L. Fragnito, and J. C. Knight, Opt. Express **16**, 2816 (2008).
7. G. Cirmi, M. Hemmer, K. Ravi, F. Reichert, L. E. Zapata, A.-L. Calendron, H. Cankaya, F. Ahr, O. D. Mucke, N. H. Matlis, and F. X. Kartner, J. Phys. B **50**, 044002 (2017).
8. D. D. Hickstein, D. R. Carlson, A. Kowligy, M. Kirchner, S. R. Domingue, N. Nader, H. Timmers, A. Lind, G. G. Ycas, M. M. Murnane, H. C. Kapteyn, S. B. Papp, and S. A. Diddams, Optica **4**, 1538 (2017).
9. N. An, H. Ren, Y. Zheng, X. Deng, and X. Chen, Appl. Phys. Lett. **100**, 221103 (2012).
10. C. Chen, C. He, D. Zhu, R. Guo, F. Zhang, and S. Pan, Opt. Lett. **38**, 3137 (2013).
11. A. S. Kowligy, A. Lind, D. D. Hickstein, D. R. Carlson, H. Timmers, N. Nader, F. C. Cruz, G. Ycas, S. B. Papp, and S. A. Diddams, Opt. Lett. **43**, 1678 (2018).
12. C. Bosshard, R. Spreiter, M. Zgonik, and P. Günter, Phys. Rev. Lett. **74**, 2816 (1995).
13. R. Debnath, S. K. Beda, and A. Saha, Optik **138**, 256 (2017).
14. Y. Qin, Y. Zhu, S. Zhu, and N. Ming, J. Phys. Condens. Matter **10**, 8939 (1998).
15. G. Li, Y. Chen, H. Jiang, and X. Chen, Photonics Res. **3**, 168 (2015).
16. A. Boes, B. Corcoran, L. Chang, J. Bowers, and A. Mitchell, Laser Photonics Rev. **12**, 1700256 (2016).
17. A. J. Mercante, D. L. K. Eng, M. Konkol, P. Yao, S. Shi, and D. W. Prather, Opt. Lett. **41**, 867 (2016).
18. C. Wang, M. Zhang, B. Stern, M. Lipson, and M. Lončar, Opt. Express **26**, 1547 (2018).
19. C. Wang, M. Zhang, X. Chen, M. Bertrand, A. Shams-Ansari, S. Chandrasekhar, P. Winzer, and M. Lončar, Nature **562**, 101 (2018).
20. L. Chang, Y. Li, N. Volet, L. Wang, J. Peters, and J. E. Bowers, Optica **3**, 531 (2016).
21. M. Chauvet, F. Henrot, F. Bassignot, F. Devaux, L. Gauthier-Manuel, V. Pecheur, H. Maillotte, and B. Dahmani, J. Opt. **18**, 085503 (2016).
22. R. Luo, Y. He, H. Liang, M. Li, and Q. Lin, Optica **5**, 1006 (2018).
23. N. Courjal, B. Guichardaz, G. Ulliac, J.-Y. Rauch, B. Sadani, H.-H. Lu, and M.-P. Bernal, J. Phys. D **44**, 305101 (2011).
24. N. Courjal, F. Devaux, A. Gerthoffer, C. Guyot, F. Henrot, A. Ndao, and M.-P. Bernal, Opt. Express **23**, 13983 (2015).
25. J.-W. Zhao, C.-P. Huang, Z.-Q. Shen, Y.-H. Liu, L. Fan, and Y.-Y. Zhu, Appl. Phys. B **99**, 673 (2010).
26. Y. Lu, Z. Wan, Q. Wang, Y. Xi, and N. Ming, Appl. Phys. Lett. **77**, 3719 (2000).
27. T. Ding, Y. Zheng, and X. Chen, J. Lightwave Technol. (2019) (in press).
28. S. Kurimura, Y. Kato, M. Maruyama, Y. Usui, and H. Nakajima, Appl. Phys. Lett. **89**, 191123 (2006).
29. L. Wang, C. E. Haunhorst, M. F. Volk, F. Chen, and D. Kip, Opt. Express **23**, 30188 (2015).
30. C. Wang, C. Langrock, A. Marandi, M. Jankowski, M. Zhang, B. Desiatov, M. M. Fejer, and M. Lončar, Optica **5**, 1438 (2018).